Mesitylthio-Oligothiophenes in Various Redox States. Molecular and Electronic Views as Offered by Spectroscopy and Theory

Juan Casado

Department of Physical Chemistry, University of Málaga, Campus de Teatinos s/n, Málaga 29071, Spain

Marek Z. Zgierski

Steacie Institute for Molecular Sciences, National Research Council of Canada, K1A 0R6, Ottawa, Canada

Robin G. Hicks and Daniel J. T. Myles

Department of Chemistry, University of Victoria, P.O. Box3065 Victoria, British Columbia V8W 3V6, Canada

Pedro M. Viruela and Enrique Ortí*

Institut de Ciència Molecular, Universitat de València, Doctor Moliner 50, Burjassot 46100, Spain

M. Carmen Ruiz Delgado, Víctor Hernández, and Juan T. López Navarrete*

Department of Physical Chemistry, University of Málaga, Campus de Teatinos s/n, Málaga 29071, Spain

Received: May 26, 2005; In Final Form: October 6, 2005

A series of α,ω-bis(mesitylthio)oligothiophenes of various chain lengths and with different side substitution patterns have been studied in their oxidized states by means of electron absorption and Raman spectroscopies in combination with theory in the framework of the density functional theory. Upon chemical oxidation, stable radical cations, dications, and even radical trications are generated. Longer chain lengths better stabilize higher oxidation states. The tetramer can be easily converted to the dication, and a trication can be obtained for the ethylenedioxy derivative. The α,ω-sulfur atoms are actively involved in the formation of the charged species and exert a favorable tuning of their electronic structure. Raman spectra provide experimental evidence of the attainment of quinoidal structures within the conjugated path, initially heteroaromatic, with different extension as a function of the *p*-doping level.

I. Introduction

Molecular electronics promises to use single molecules as the basic operational component in future computational architectures.[1−7] Detailed understanding of electron transport through a molecule bridging a gap between two metal electrodes is essential for the development of this emerging technology. Particularly, there exists a large interest in π-conjugated molecules of defined length and constitution to act as molecular wires in these molecular-scale devices. Electron transport through single-molecule junctions is determined by the local electronic structure of this nanoscale region including the molecule. This structure is also strongly affected by the perturbation of the molecule/metal contacts, which therefore play a key role. Transport phenomena reported for molecular junctions include negative differential resistance,[8] rectification,[9] conductance quantization,[10] and switching.[1,2,11]

The excellent physical and chemical properties of oligothiophenes provide one of the most attractive fields of research concerning conjugated molecules to which very intense research activity is being presently devoted. Oligothiophenes are viewed as rich electron systems, because of their outstanding ability to accommodate positive charges and to transport them through self-assembled monolayers or thin films. These features are highly desirable in electronic applications, and many examples of devices using oligothiophenes as the semiconductor element have been presented: field-effect transistors (FET),[12−15] light-emitting diodes (LED),[16−18] and so forth.

One of the most fruitful ways to bond organic molecules to metal surfaces is by means of thiol-terminated groups.[1,2,19,20] In this sense, it is instructive to analyze molecular wires based on oligothienylene systems functionalized with thioether (−S−) groups that might potentially mimic the wire connection to the surface of the "bulk" medium. As a first step for the whole analysis of this configuration, this work focuses on the interaction of the conjugated wire and the S alligator addressed in free molecules in solution. These molecules are oligothiophenes of sizable length which have their two terminal positions substituted with mesitylthio groups (see Figure 1). Within the context of molecular electronics, studies on the structure of charged oligothiophenes are relevant to hole transport through single molecules, since this process can be regarded as the result of the *p*-doping of the *semiconducting* molecule. Since the *p*-doped molecule becomes the ultimate responsible of charge transport, it is of great significance to analyze the dependence of its electronic structure with (a) the size of the thiophene backbone, (b) the thioether substitution, and (c) the presence of end mesityl

* To whom correspondence should be addressed. E-mail: (J.T.L.N.) teodomiro@uma.es.

10.1021/jp052778i CCC: $30.25
Published on Web 11/15/2005

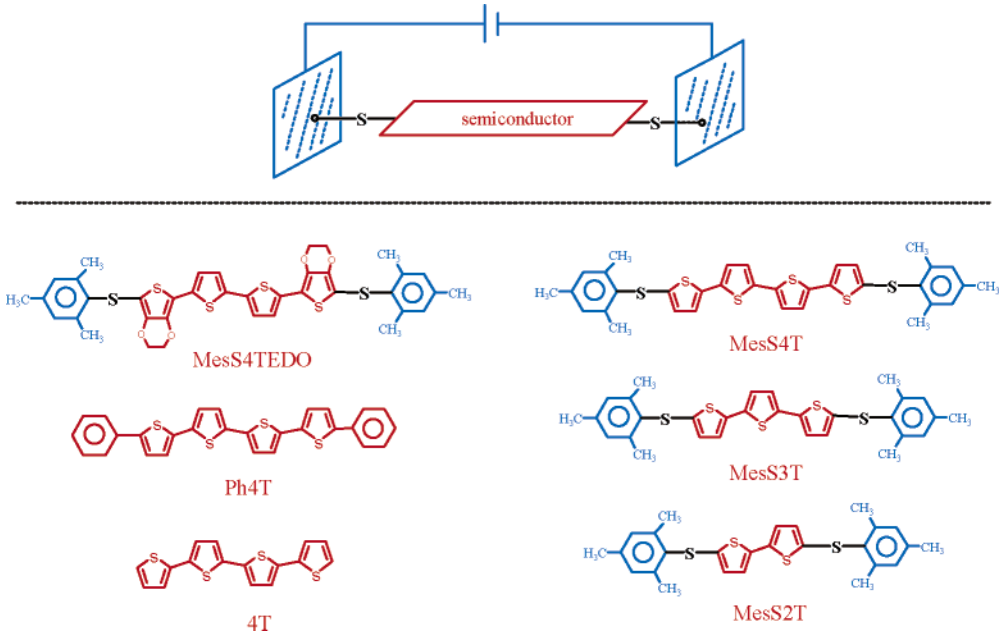

Figure 1. Scheme of a single-molecule device and chemical structures of representative molecules for the semiconductor element.

rings. Mesityl moieties here replace the bulk medium to which oligothiophene wires are bonded.

Our objective is to explore the structure and electronic properties of these oxidized oligothiophenes, making emphasis on how the charging process affects the mesityl → oligothiophene −S− connections and the conjugated chain itself as the element supporting the charge current. In this regard, the paper is intended to provide valuable information about conjugated molecular systems that could be successfully employed in molecular electronics. To this end, a suitable combination of experimental spectroscopic (UV−vis−near-IR electron absorption and vibrational Raman spectroscopies) and quantum chemical methods are used.

Among the reasons for the use of Raman spectroscopy, it is to be mentioned that this tool is established to be a highly sensitive indicator of conjugation or π-electron delocalization in organic molecules, which, otherwise, is the most relevant feature of the electronic structure of oligothiophenes.[21−23] Conjugation extension, either for neutral or quinoid structures (inversion of the C═C/C−C aromatic pattern), leads to an intensification of particular lines corresponding to symmetric stretching vibrations of the bonds forming the C═C/C−C alternating sequence of the conjugated path and to a decrease of their associated Raman frequencies. Particular attention must be paid to quinoidization, because it is the relevant structural and electronic feature governing the mechanism of oxidative doping of this class of organic molecules.[21,24,25]

II. Experimental and Theoretical Details

Spectroscopic studies and synthetic details for these molecules in their neutral state have been previously reported.[22,26] The chemical structures and nomenclature of some representative molecules are depicted in Figure 1. It follows that MesS2T and MesS3T deal respectively with the systems with two and three thiophene rings, 4T with the unsubstituted tetrathiophene, Ph4T with quaterthiophene end-capped with two phenyl rings, and so on. Chemical oxidations were effected by using iron(III) chloride ($FeCl_3$). The oligothiophenes and $FeCl_3$ fresh solutions were prepared in dry degassed dichloromethane (99.9% from Aldrich). Oxidations were carried out by stepwise mixing of both solutions followed by in situ recording of the spectra. UV−vis−near-IR data were obtained on a Perkin-Elmer Lambda 19 UV−vis−near-IR apparatus. FT-Raman spectra were measured using an FT-Raman accessory kit (FRA/106-S) of a Bruker Equinox 55 FT-IR interferometer. A continuous-wave Nd:YAG laser working at 1064 nm was employed for excitation. A germanium detector operating at liquid nitrogen temperature was used. Raman scattering radiation was collected in a backscattering configuration with a standard spectral resolution of 4 cm^{-1}. To avoid possible damage to the oxidized samples, laser power was kept at a level lower than 100 mW and 1000−3000 scans were averaged for each spectrum.

Density functional theory (DFT) calculations were carried out by means of the *Gaussian 98* program[27] running on SGI Origin 2000 supercomputers. We used the Becke's three-parameter exchange functional combined with the LYP correlation functional (B3LYP).[28] It has already been shown that the B3LYP functional yields similar geometries for medium-sized molecules, as MP2 calculations do with the same basis sets.[29,30] Moreover, the DFT force fields calculated using the B3LYP functional yield vibrational spectra in very good agreement with experiments.[31,32] We also made use of the standard 6-31G** basis set.[33] Optimal geometries were determined on isolated entities. All geometrical parameters were allowed to vary independently. On the resulting ground-state optimized geometries, harmonic vibrational frequencies and Raman intensities were calculated analytically with the B3LYP functional. Calculated harmonic vibrational frequencies were uniformly scaled down by a factor of 0.96, as recommended by Scott and Radom.[31] All theoretical vibrational frequencies quoted in the text are thus scaled values. Radical cations were treated as open-shell systems and were computed using spin-unrestricted UB3LYP wave functions. The maximun value obtained for S^2 was 0.76, very close to the 0.75 theoretically expected for a doublet, showing that spin contamination is almost absent. Neither solvent nor counteranion effects were considered in the calculations.

Vertical electronic excitation energies were computed by using the time-dependent DFT (TDDFT) approach.[34,35] The 20 lowest-energy electronic excited states were at least computed

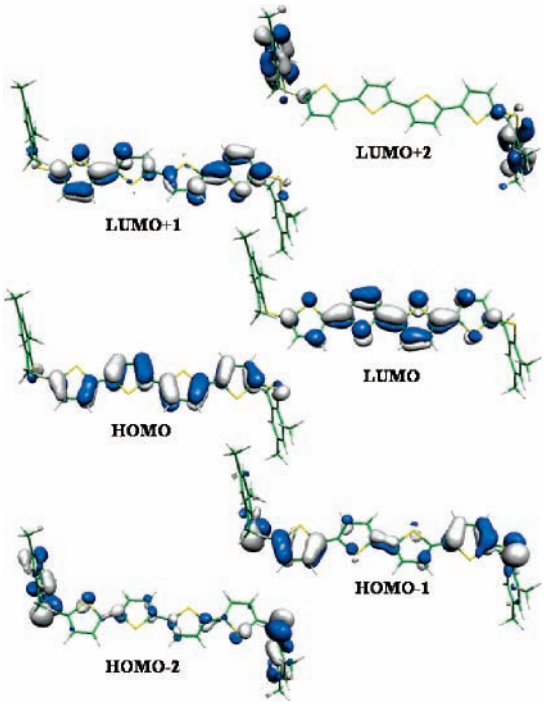

Figure 2. Electron density contour (0.03 e/bohr^3) calculated for selected molecular orbitals of MesS4T at the B3LYP/6-31G** level.

for all the molecules. The computational cost of TDDFT is roughly comparable to that of single-excitation theories based on a Hartree−Fock (HF) ground state, such as single-excitation configuration interactions (CIS). Numerical applications reported so far indicate that the TDDFT formalism employing current exchange-correlation functionals performs significantly better than HF-based single-excitation theories for the low-lying valence excited states of both closed-shell and open-shell molecules.[36,37] TDDFT calculations were carried out using the B3LYP functional and the 6-31G** basis set on the previously optimized molecular geometries obtained at the same level of calculation.

III. Electronic Spectra of the *p*-Doped Species

A. Singly Oxidized Compounds. The UV−vis spectra of neutral MesS2T, MesS3T, and MesS4T in dichloromethane show intense bands at 358, 386, and 420 nm, respectively, which increase in intensity with the number of thiophene units.[26] TDDFT calculations predict very intense transitions at 425 nm (oscillator strength $f = 1.23$) for MesS3T and at 466 nm ($f = 1.63$) for MesS4T, which correspond to almost exclusive one-electron promotions from the HOMO to the LUMO. As shown in Figure 2, these orbitals are of π nature and mainly involve the oligothiophene backbone. The intense absorptions experimentally observed are therefore assigned to $\pi-\pi^*$ HOMO → LUMO transitions. Theoretical calculations reproduce the bathochromic shift of the $\pi-\pi^*$ band with the length of the oligomer but slightly underestimate the energy of the band. This underestimation can be due to the fact that B3LYP calculations predict almost planar structures for the oligothiophene backbone in MesS3T and MesS4T (the maximum torsion angles being 9.3° and 17.0°, respectively), and more twisted structures can be present in solution. Planar structures favor electron delocalization along the carbon−carbon (CC) conjugated path and narrows the HOMO−LUMO energy gap. Previous studies have shown that DFT calculations underestimate the twisting angle in 2,2′-bithiophene.[37]

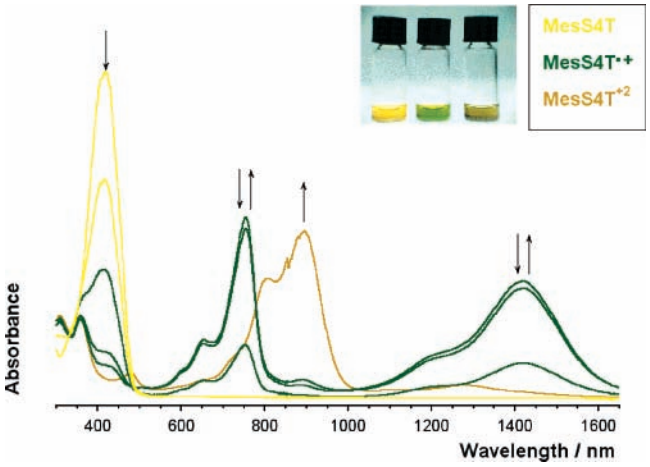

Figure 3. UV−vis−near-IR spectra of MesS4T in dichloromethane recorded after successive additions of $FeCl_3$. The insert shows the color of the oxidized samples.

The attachment of MesS groups to both ends of the tetrathiophene (4T) chain pushes up/down the HOMO/LUMO energies from −4.97/−1.94 eV in 4T to −4.93/−1.99 eV in MesS4T due to the additional conjugation effect coming from the MesS sulfur atoms that predominates over the positive electron induction. A similar HOMO/LUMO destabilizing/stabilizing effect due to the extension of conjugation is observed with increasing chain length, −5.02/−1.82 eV in MesS3T and −4.93/−1.99 eV in MesS4T. Finally, the evolution of the $\pi-\pi^*$ band from 420 nm in MesS4T to 442 nm in MesS4TEDO might be due to the hyperconjugation effect coming from the oxygen atoms through their electron lone pairs.

As the long element of the series, let us use the theoretical calculations on MesS4T$^{\bullet+}$ to assign the spectroscopic features experimentally observed. It is to be noted that the HOMO in MesS4T$^{\bullet+}$ is now singly occupied and, according to the terminology used in the field of conducting polymers, it is named as P1, where P refers to a polaron level, while P2 corresponds to the empty LUMO as shown in Scheme 1. Figure 3 displays the UV−vis−near-IR spectra of MesS4T obtained after successive addition of small amounts of $FeCl_3$. Upon oxidant addition, the band of the neutral molecule at 420 nm progressively disappears and two new bands appear at 756 and 1420 nm (1.64 and 0.87 eV, respectively). Calculations assign the experimental band at 756 nm to the intense transition calculated at 1.91 eV ($f = 1.58$), which mainly arises from a one-electron P1 → P2 excitation. The lowest-energy band at 1420 nm is related with the electronic transition to the first excited state calculated at 1.03 eV ($f = 0.40$), which results from the HOMO → P1 monoexcitation mixed with an important contribution of the P1 → P2 promotion.

The absorption bands show high-energy components at 601 and 654 nm and at 1190 nm, respectively, likely due to vibronic structure, since the differences between them fall in the range of vibrational energies: 756 → 654 nm (2063 cm^{-1}), 654 → 601 nm (1348 cm^{-1}), and 1420 → 1190 nm (1361 cm^{-1}). As discussed below, one of the strongest Raman lines is measured at 1382 cm^{-1}, reinforcing this assignment.[38−40] These bands show neither concentration nor solvent polarity dependence, and cannot be assigned to π-dimeric species. The formation of these species through cofacial coupling of two free radical cations seems to be precluded by the steric hindrance of the two mesityl groups. Indeed, B3LYP/6-31G** calculations predict that the most stable conformation of MesS4T$^{\bullet+}$ corresponds to a C_{2h} structure in which the quaterthiophene backbone is fully planar

SCHEME 1: Energy Diagram Showing the New Levels (in red) Appearing in the Gap for a Positive Polaron (P) and a Positive Bipolaron (BP) Regarding the Neutral Form

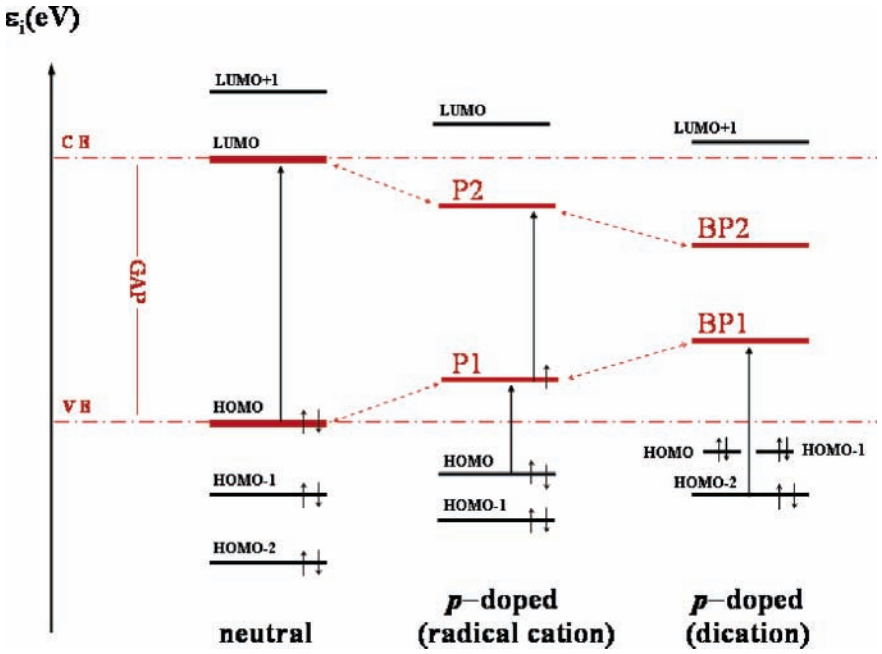

and the mesityl groups are perpendicular to the molecular plane. The occurrence of these structured bands in the electronic absorption spectrum has therefore to be ascribed to vibronic progressions due to specific vibrational normal modes.[41−46]

Figure 4 displays the spectra of the radical cations of MesS2T, Ph3T, MesS3T, 4T, Ph4T, MesS4T, and MesS4TEDO obtained after treatment with $FeCl_3$. A shift to lower energies of the main absorption features is observed with increasing chain lengths: 572 and 905 nm for $MesS2T^{\bullet+}$, 676 and 1170 nm for $MesS3T^{\bullet+}$, and 756 and 1420 nm for $MesS4T^{\bullet+}$. The involvement of more delocalized molecular orbitals for the longer oligomers (see Figure 2) explains the dependence of the energy of the bands with the number of rings.

The spectrum of $4T^{\bullet+}$ displays two main bands measured at 651 and 1071 nm of the same nature as those already discussed for $MesS4T^{\bullet+}$. Again, the active participation of the MesS sulfurs in the conjugated path is the reason for the shift to lower energies observed for the two bands in $MesS4T^{\bullet+}$ (0.26 and 0.28 eV, respectively) with respect to nonsubstituted $4T^{\bullet+}$. The radical cation of MesS4TEDO shows two intense bands at 769 and 1442 nm, each one accompanied by weak vibronic features

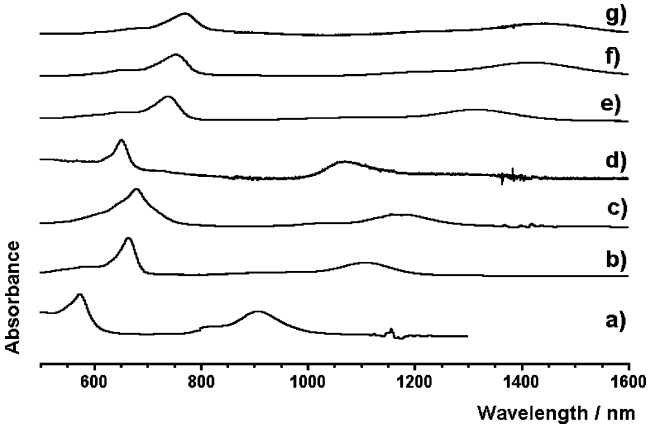

Figure 4. Vis−near-IR spectra of (a) $MesS2T^{\bullet+}$, (b) $Ph3T^{\bullet+}$, (c) $MesS3T^{\bullet+}$, (d) $4T^{\bullet+}$, (e) $Ph4T^{\bullet+}$, (f) $MesS4T^{\bullet+}$, and (g) $MesS4TEDO^{\bullet+}$ in dichloromethane.

at 687 and 1267 nm, respectively. The slight red shifts (0.01 and 0.03 eV) of the $MesS4TEDO^{\bullet+}$ bands relative to those of $MesS4T^{\bullet+}$ must concern with the positive inductive effect coming from the electron lone pairs of the oxygen atoms toward the π-conjugated spine that help to balance the introduction of one positive charge over the π skeleton. The greater band displacements found for the $4T^{\bullet+} \rightarrow MesS4T^{\bullet+}$ structural modification compared with the $4T^{\bullet+} \rightarrow MesS4TEDO^{\bullet+}$ modification show a more effective electronic intervention of the sulfur atoms at the end-capping α positions than of the oxygen atoms at β. This is likely due to the larger polarizability of the electron lone pairs of the sulfur atoms versus those of the oxygen atoms and to the more effective interaction of the α-substituents with the conjugated spine.

It is also interesting to compare the electron absorption features of $Ph3T^{\bullet+}$ and $MesS3T^{\bullet+}$ to analyze the role played by the MesS sulfur atoms. In principle, Ph3T can be regarded as a parent system of MesS3T lacking C−S bridges, and one could think that Ph3T/MesS3T comparisons might be suitable to account for the particular electronic effects of the electrode connecting −S− groups. Unfortunately, this is not the case, because the phenyl caps in Ph3T are almost coplanar with the oligothienylene spine and actively participate in the conjugation path of the molecule, which is far from the idea of the phenyl groups acting as perpendicular electrodes.[47,48] The similar energies found for the two electronic absorptions of $MesS3T^{\bullet+}$ (676 and 1170 nm) and $Ph3T^{\bullet+}$ (664 and 1107 nm) are in fact due to different reasons. For $MesS3T^{\bullet+}$, the mesityl groups are perpendicular to the oligothienylene chain, and only the sulfur atoms are involved in the conjugation path. For $Ph3T^{\bullet+}$, the phenyl groups contribute to the extension of the delocalized π-system and determine the relatively low excitation energies found for this compound.

B. Doubly Oxidized Compounds. Stepwise addition of 2 equiv of $FeCl_3$ to the solution of neutral MesS4T gives rise to the clearance of the bands associated with the neutral and radical cation forms and to the appearance of new bands belonging to the dicationic species $MesS4T^{2+}$ (see Figure 3). The vis−near-IR spectrum of $MesS4T^{2+}$ is presented in Figure 5 together with

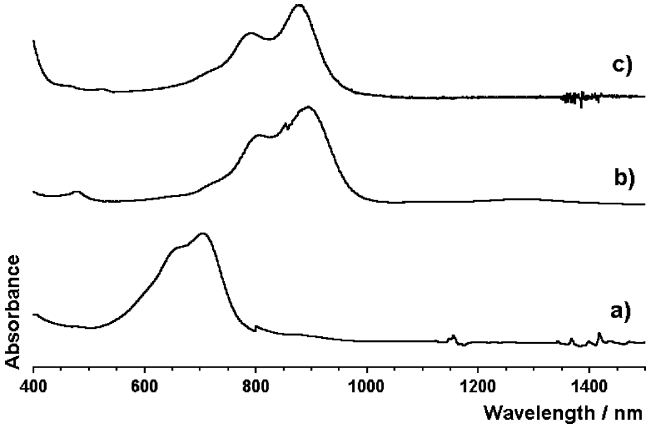

Figure 5. Vis−near-IR spectra of (a) MesS3T^{+2}, (b) MesS4T^{+2}, and (c) MesS4TEDO^{+2} in dichloromethane.

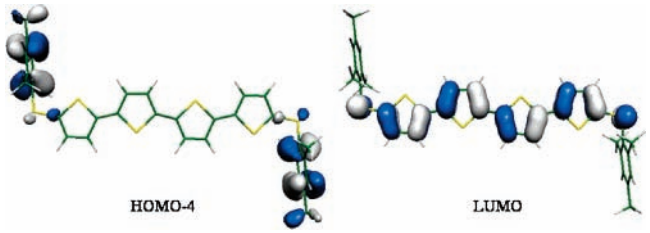

Figure 6. Electron density contours (0.03 e/bohr^3) calculated for the HOMO−4 and LUMO orbitals of MesS4T^{2+} at the B3LYP/6-31G** level. The LUMO of MesS4T^{2+} corresponds to the BP1 level in Scheme 1.

those of MesS3T^{2+} and MesS4TEDO^{2+}. It is characterized by a very intense band at 885 nm (1.40 eV) with a vibronic peak on its high-energy side measured at 802 nm (difference of 1209 cm^{-1}). According to TDDFT calculations for MesS4T^{2+}, the absorption band is due to the very intense HOMO−2 → LUMO (BP1 level in Scheme 1) one-electron promotion calculated at 716 nm (1.73 eV, $f = 2.43$), which corresponds to a $\pi-\pi^*$ transition mainly involving the oligothiophene chain and the thioether sulfurs. Two minor bands are also observed experimentally at 1277 and 479 nm. The latter band is related with the theoretical feature calculated at 441 nm ($f = 0.14$). Calculations predict the occurrence of a very low intensity transition at 1131 nm (1.10 eV, $f = 0.003$) that could be the origin of the band observed at 1277 nm (0.97 eV). The transition implies an electron transfer from the HOMO−4 level, mostly located on the two terminal mesityl groups, to the LUMO level, that spreads almost proportionally over the whole CC conjugated path (see Figure 6). The low intensity of the transition results from the almost negligible overlap between the two orbitals involved because of the perpendicular disposition of the mesityl and oligothiophene π-systems. It is to be mentioned that the HOMO, HOMO−1, and HOMO−3 orbitals of MesS4T^{2+} are also localized over the benzene rings and give rise to low-energy transitions that are dipole-forbidden or have no intensity ($f < 0.0001$).

MesS3T^{2+} is also experimentally accessible by chemical treatment with $FeCl_3$, which is not the case of MesS2T^{2+}. The electronic absorption spectrum of MesS3T^{2+} displays one very intense band at 696 nm, which is theoretically predicted at 607 nm ($f = 1.64$), with an important shoulder at 654 nm. The assignment of the absorption band is similar to that performed for MesS4T^{2+}, and the bathochromic shift observed in passing to the tetramer is related with the delocalized character of the π-orbitals involved in the transition, which extend over the entire oligothiophene spine up to the thioether sulfurs connecting the mesityl groups.

While the dicationic species of the unsubtituted parent 4T^{2+} quickly decomposes by chemical degradation, MesS4TEDO is easily oxidized up to the trication species. Similarly to MesS4T^{2+}, the spectrum of MesS4TEDO^{2+} consists of an intense band at 876 nm with a vibronic peak at 791 nm. Opposite to what is found for the radical cation, the introduction of EDO groups slightly blue-shifts the bands of the dication with respect to MesS4T^{2+} (885 and 802 nm). In contrast, the dication of the MesS4T derivative bearing EDO groups on the two innermost thiophene rings shows the subgap absorption at 900 nm, red-shifted relative to MesS4T^{2+}. This different behavior is due to the electrostatic interaction between the MesS sulfurs and the EDO oxygens that are in adjacent positions for MesS4TEDO. The presence of the EDO groups accounts for the attainment of a third stable oxidation state in MesS4TEDO that likely corresponds to the stabilization of a trication. The vis−near-IR spectrum of this species is characterized by one medium-intensity band at 710 nm with a vibronic structure at 652 nm. There is a second band at 1238 nm, which would complete the two-bands pattern characteristic of the open-shell electronic structure of the radical species that is expected upon removing one electron from the closed-shell dication.

IV. Raman Spectra and Molecular Structures of the *p*-Doped Species

The origin and magnitude of the Raman intensity are well-established to depend on the conditions of the Raman experiment and, in particular, of the energy used for the laser excitation. Resonant Raman conditions are reached when the energy of the laser line coincides with the electronic absorption. In this situation, the scattering intensity associated with a given chromophore can be enhanced by factors going from 10^3 to 10^6.[51] Hence, one cannot exclude some dependence of the Raman profile for the oxidized forms of our compounds on the experimental conditions, especially for the radical cations, given that a 1064-nm excitation was used in all cases.

A. Singly Oxidized Compounds. Let us revise the Raman spectra of the neutral systems for comparison purposes. It has been previously established that the Raman bands observed for conjugated oligomers are due to collective stretching vibrations of the C═C/C−C conjugated path, for which the atomic displacements produce the largest changes of the molecular polarizability as a consequence of the occurrence of a very effective *electron−phonon* mechanism (ECC theory in last section of this paper).[24,25,52] The Raman spectrum of neutral MesS4T (Figure 7) is dominated by two main bands at 1515 (line A) and 1454 cm^{-1} (line B), which originate in two stretching C═C/C−C modes mainly located, respectively, on the two outer and two inner thiophene rings.[22] Figure 8 depicts the eigenvector of the vibrational normal mode associated with the Raman band at 1454 cm^{-1}. One of the main terms in the equation of the Raman intensity arises from the transition dipole moments summed over all the electronic states of the molecule.[51] For the neutral molecule, the Raman spectrum is obtained in off-resonant conditions, and according to the two-states model, the largest contribution to the dipolar moment term is expected to emerge from the most intense band of the electronic absorption spectrum, i.e., the $\pi-\pi^*$ band associated with the HOMO−LUMO excitation. Since these two orbitals are more concentrated in the central part of the molecule, the two inner rings contribute more to the transition dipole moment, which would explain the higher Raman intensities found for the

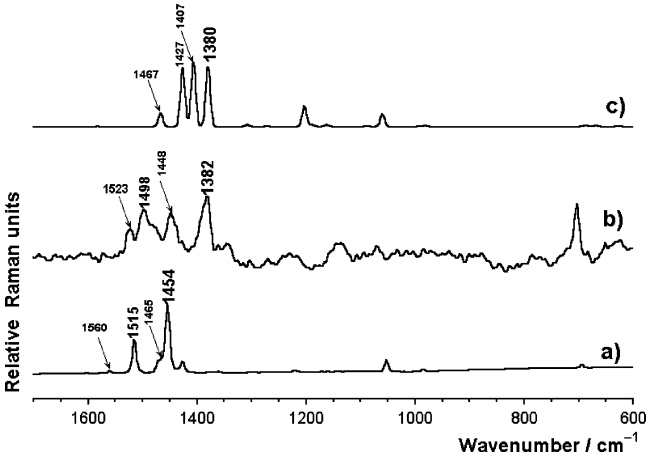

Figure 7. Comparison among (a) Raman spectrum of neutral MesS4T in solid state, (b) Raman spectrum of MesS4T$^{\bullet+}$ in dichloromethane solution, and (c) UB3LYP/6-31G** Raman theoretical spectrum of MesS4T$^{\bullet+}$.

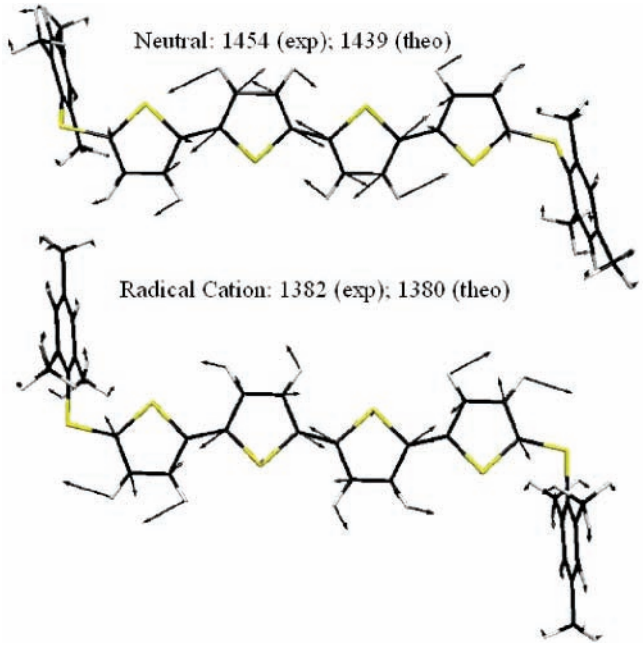

Figure 8. Vibrational eigenvectors associated with the most intense bands of the Raman spectra of MesS4Tand MesS4T$^{\bullet+}$. Experimental and calculated wavenumbers are given in reciprocal centimeters.

vibrational modes with the largest atomic motions in the center of the molecule as line B in detriment of line A.

The generation of the radical cation gives rise to the disappearance of the Raman scatterings of the neutral form and to the appearance of new lines all shifted to lower-frequency values. As shown in Figure 7, four intense Raman bands merge for MesS4T$^{\bullet+}$ at 1523, 1498, 1448, and 1382 cm^{-1}. The theoretical Raman spectrum calculated for MesS4T$^{\bullet+}$ also predicts the appearance of four intense bands in the range 1520−1380 cm^{-1}. The lowest-energy component is calculated at 1380 cm^{-1}, in good accord with the strongest scattering observed at 1382 cm^{-1}, and its associated eigenvector is depicted in Figure 8. Medium-intensity bands are recorded at 1232, 1140, and 1070 cm^{-1} and can be correlated with those calculated at 1203, 1162, and 1060 cm^{-1}. The intense feature at 700 cm^{-1} is due to the solvent. The UB3LYP/6-31G** Raman spectrum of MesS4T$^{\bullet+}$ is also shown in Figure 7, and the eigenvectors associated to the most important Raman lines of the theoretical UB3LYP/6-31G** Raman spectrum of MesS4T$^{\bullet+}$ are shown in Figure 8.

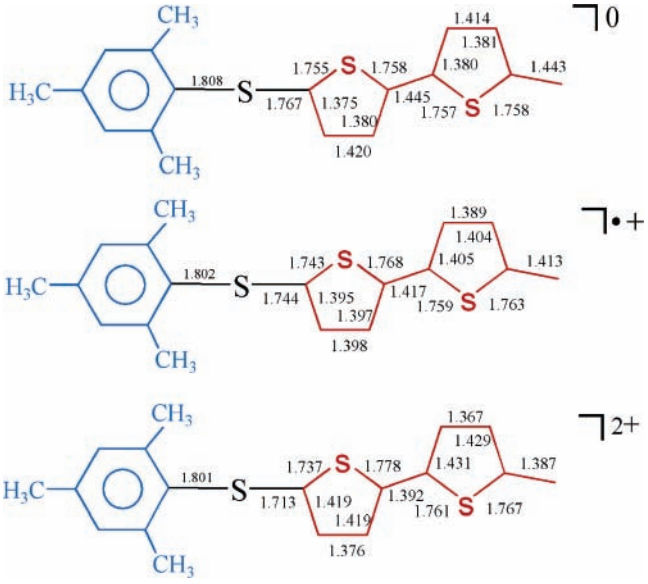

Figure 9. B3LYP/6-31G** bond distances (in Å) calculated for neutral MesS4T, MesS4T$^{\bullet+}$, and MesS4T^{+2}.

The average of the differences between the lengths of successive single and double CC bonds defines the bond length alternation (BLA) pattern and is taken as a measure of the π-electron delocalization in the conjugated path. A decrease of the BLA value is associated with an increasing degree of π-electron delocalization or skeletal relaxation along the conjugated path and produces a wavenumber softening of the C═C/C─C stretching modes. Figure 9 summarizes the evolution of the main structural data on going from neutral MesS4T to the charged species. Upon one-electron extraction, the BLAs of the external/internal thiophene rings change from 0.043/0.034 Å in MesS4T to 0.002/−0.015 Å in MesS4T$^{\bullet+}$ (the minus sign in the latter BLA value is introduced to stress the inversion from an aromatic (positive sign) to a quinoid pattern (negative sign)). Thus, an aromatic to quinoid inversion of the structural pattern takes place in the central rings, and an equalization of the CC bonds occurs for the outer rings. The larger BLA change calculated for the central part of the molecule agrees well with the larger wavenumber shift measured for line B, 72 cm^{-1}, and with the more modest changes observed for the lines located at the outermost rings, 1560 → 1523 cm^{-1} and 1514 → 1498 cm^{-1}. However, it must be stressed that these modes are not ring-localized vibrations but collective motions also involving the stretching of the inter-ring CC bonds (see Figure 8). The lengths of these bonds (outer/inner) strongly change in passing from MesS4T (1.445/1.443 Å) to MesS4T$^{\bullet+}$ (1.417/1.413 Å) and become structural markers of the increasing quinoid character of the whole tetrathiophene chain. It must be noted that for the related system α,α′-dimethylquaterthiophene (DM4T) the strongest Raman line (line B) appears at 1482 cm^{-1} and shifts down by 67 cm^{-1} to 1415 cm^{-1} in the radical cation.[53] In comparison to DM4T, line B in MesS4T is measured at lower frequencies (∼30 cm^{-1}) both for the neutral molecule (1454 cm^{-1}) and for the radical cation (1382 cm^{-1}). This result stresses that the downshift observed for the position of line B in the Raman spectrum of MesS4T is due to the extra conjugation provided by the thioether sulfurs and confirms that these atoms actively interact with the conjugation path of the oligothiophene chain.

The effective inter-ring π-electron delocalization, both in neutral and in radical cation forms, balances the weak aromatic character of the thiophene rings and determines that the S atoms of the oligothiophene act as mere electron donors toward the

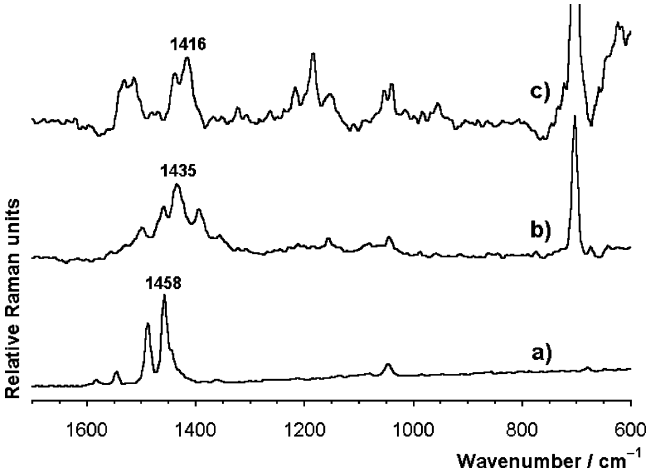

Figure 10. Comparison of the Raman spectra recorded for neutral MesS4TEDO in the solid state (a) and for MesS4TEDO$^{\bullet+}$ (b) and MesS4TEDO^{2+} (c) in dichloromethane solution.

positively charged C═C/C—C chain. The MesS sulfurs actively participate in the conjugated path and accumulate an extra charge of +0.25 e, i.e., one-fourth of the whole injected charge, revealing the remarkable role they play in the oxidative doping. This participation is structurally reflected in the C—S bonds connecting the mesityl S atoms to the oligothiophene chain, which largely shorten by 0.023 Å, while its C—S counterparts toward the mesityl groups only change by 0.006 Å, indicating the minimal involvement of the electrode-like moieties. The scenario is different for the thienyl C—S bonds. They slightly lengthen upon charge injection with the exception of the C—S bonds contiguous to the end-capping α-positions, which unexpectedly shorten (see Figure 9). The fact that the thiophene sulfurs contribute to the stabilization of the positive charge but are not involved in the conjugation path explains why the Raman bands associated with the stretching of their bonds are not observed. For the same reason, the bands belonging to the mesityl groups are not observed, because their perpendicular disposition relative to the oligothiophene chain precludes charge delocalization and thus remains mainly unaffected upon oxidation.

On going from MesS4T$^{\bullet+}$ to MesS3T$^{\bullet+}$, Raman bands are slightly displaced to lower wavenumbers (1523 → 1512 (shoulder) cm^{-1}, 1498 → 1492 cm^{-1}, and 1448 → 1443 cm^{-1}), except for the 1382 → 1386 cm^{-1} couple. This effect is due to the larger quinoidization of the oligothiophene structure that takes place in the shorter oligomer as revealed by the larger BLA, in absolute value, obtained for the central thiophene rings in MesS3T$^{\bullet+}$ (−0.021 Å) as compared with MesS4T$^{\bullet+}$ (−0.015 Å). The larger geometrical distortion calculated for MesS3T$^{\bullet+}$ also affects the C—S bonds connecting the mesityl groups to the terthiophene chain, which shorten by 0.029 Å (0.023 Å in the tetramer).

B. Doubly Oxidized Compounds. The relative proximity to the 1064-nm laser line of the very intense electronic band of the MesS4T^{2+} species and its associated fluorescence impeded the Raman measurements. In contrast, the Raman spectrum of the dication of MesS4TEDO was obtained without much difficulty. This could be concerned with the fluorescence deactivation through space inter- and intramolecular S···O interactions that could promote other deactivation mechanisms. Figure 10 displays the Raman profiles recorded for the neutral and oxidized species of MesS4TEDO. Force field and Raman intensity calculations were carried out for the three oxidation states. Structural data show the same trends discussed above

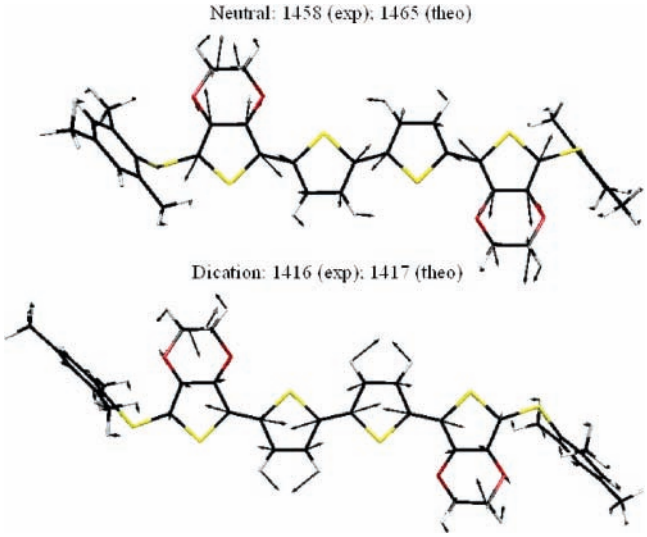

Figure 11. Vibrational eigenvectors associated with the strongest Raman bands of the spectra of MesS4TEDO and MesS4TEDO^{2+}. Experimental and theoretical values are given in reciprocal centimeters.

for the radical cation of MesS4T. As shown in Figure 9 for MesS4T, two-electron extraction fully inverts the aromatic geometry of the neutral oligomer to a quinoid structure, in which the BLA patterns of the four thiophene rings are now negative and all single CC bonds in the neutral molecule have now double-bond character and vice versa. We looked at the Raman spectra for experimental evidence of this theoretical prediction. The strongest Raman line, which corresponds to a collective stretching vibration of the C═C/C—C path, is recorded at 1458 cm^{-1} in neutral MesS4TEDO and progressively shifts to 1435 cm^{-1} in MesST4EDO$^{\bullet+}$ and to 1416 cm^{-1} in MesS4TEDO^{2+}. This 42-cm^{-1} displacement to lower wavenumbers is nicely accounted for by theoretical calculations, which provide a downshift of 50 cm^{-1} upon oxidation to the dication. Figure 11 sketches the vibrational eigenvectors associated with the most intense bands calculated for MesS4TEDO in neutral and dication forms. For both species, the vibration is mainly concerned with the stretching of the CC double bonds that correspond to the C_α—C_β bonds in neutral MesS4TEDO and to C_α—$C_{\alpha'}$ bonds in MesS4TEDO^{2+}. The 1435 → 1416 cm^{-1} associated with the MesST4EDO$^{\bullet+}$ → MesS4TEDO^{2+} oxidation is the experimental manifestation of the increasing quinoidization of the oligothienyl chain that occurs upon successive oxidation.

Regarding the C—S bonds, the same trends previously discussed for the MesS4T → MesST4$^{\bullet+}$ oxidation are valid for the oxidation to the dication. As shown in Figure 9, the C—S bonds connecting the mesityl groups with the oligothiophene chain undergo the largest shortening (0.031 Å) on passing to the dication, and all the thienyl C—S bonds lengthen with the exception of those nearest to the mesityl groups that shorten by 0.006 Å. In Scheme 2, a simple mechanism is proposed based on two resonant forms to explain the unexpected shortening predicted for the outermost thienyl C—S bonds on going from the neutral molecule to the radical cation and to the dication. The large involvement of the mesityl S atoms in the stabilization of the positive charges might favor, in a synergic process, the charge delocalization on their vicinal thienyl S atoms. Interestingly, this simple view suggests a change from an sp^3 hybridization of the terminal sulfurs in the neutral molecule to an sp^2 hybridization in the case of the charged species, that is more marked in the dication. Although electrostatic repulsions tend to separate the two positive charges far away in the chain, the mesityl groups remain minimally affected for the divalent

SCHEME 2: Resonant Forms Mainly Involved in the Stabilization of the Dication Species

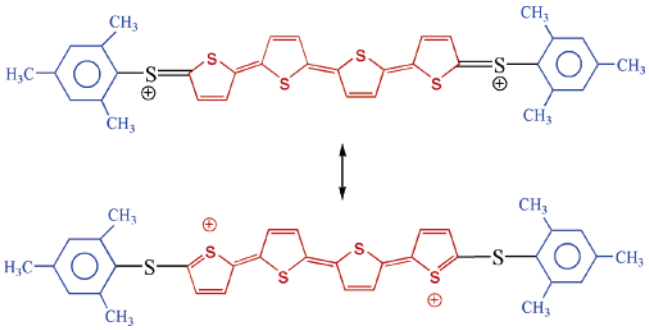

species, likely due to their perpendicular disposition regarding the central spine.

C. ECC Theory: Unified View of the Raman Spectra. If $3N - 6 = 204$ (N, number of atoms) is the total number of normal modes of MesS4T, then around 110 are Raman-active vibrations assuming the C_{2h} symmetry. Unexpectedly, only 1 very intense Raman band is observed in the spectrum of neutral MesS4T in the CC stretching region. More bands, 5 with similar intensity, are measured for its radical cation (Figure 7). Similar trends are observed for MesS4TEDO in its 3 oxidation states (Figure 10). These findings are common for the Raman spectra of all polyconjugated oligomers and polymers which offer a long delocalization pathway to the p_z electrons, as either neutral or oxidized/reduced compounds. This Raman behavior has been explained for polyacetylene by using the amplitude mode theory[52] and for oligoenes, polyacetylene, polypyrrole, polyalkylpyrroles, and polythiophenes by using the effective conjugation coordinate (ECC) theory.[24,25] The ECC theory assumes the existence of a coordinate, *Я*, that describes the path the p_z electrons follow in going from the "aromatic" ground state to the higher-energy "quinoid" state and that relates with the *electron*−*phonon* coupling terms in the electronic Hamiltonian. In the space of internal coordinates, *Я* is exclusively composed of C═C/C−C stretching modes.

A force constant ($F_Я$) associated with this conjugation coordinate can be defined and calculated. However, it is to be stressed that *Я* does not represent any normal mode, and its projection over the vibrational space defines the intensity distribution among the Raman active modes and therefore its appearance. For the neutral molecules, $F_Я$ takes high values due to the predominance of symmetric C═C intra-ring stretching modes (ring pinning of the electronic potential), while the rest of stretchings should have vanishing Raman cross-sections. As a result, only one big intense line is observed, line B, in MesS4T and MesS4TEDO. With the increment of the inter-ring delocalization of the p_z electrons or of quinoidization in the case of the oxidized species, $F_Я$ decreases (existence of negative contributions to $F_Я$ arising from CC inter-ring force constants), and the associated Raman lines now appear at lower wavenumbers and, most important to understanding the Raman profile of the oxidized samples, the value of $F_Я$ reaches those of other C═C/C−C modes less involved in the dynamics of *Я* (very weak bands in the Raman spectrum of the neutral). The straightforward consequence is that it lends part of its intensity (vibrational coupling through repulsion of vibrational levels) to other lower-energy C═C/C−C modes that now appear with appreciable intensity. In other words, the spectra of the oxidized species are characterized by the appearance of a larger number of Raman bands, all of them weaker (in relative terms) than that of the neutral and appearing at lower wavenumber values than in the nonoxidized sample. In this regard, ECC theory nicely accounts for the intensity/position of the Raman profiles on changing the aromatic pattern of the neutrals to a quinoid one in the oxidized species.

V. Summary and Conclusions.

In the field of molecular electronics, there exists a growing interest in the knowledge of the physicochemical properties of single-molecule devices constituted by a molecular wire (i.e., conjugated molecule) suitably connected to a bulk surface (i.e., metal electrode). This paper mainly focuses on the mutual affectation between the conjugated wire (i.e., oligothienylene chain) and the −S− alligator clip function. The study of this portion outlines the relevant influence of the thiol group on the electronic properties of the conjugated wire and would necessarily precede a further attempt to understand the role of the bulk/surface effects. For this purpose, the study of α,ω-bis(mesitylthio)oligothiophenes, here investigated in solution, can be highly informative about the effects of the covalent connection of a conjugated wire to a −S− alligator clip. Our motivation deals with the charged species, since the efficiency of the on (charging)/off (discharging) switching through this physical configuration involves the accommodation of positive charges within the molecular framework. The structural dependence on (i) the size of the conjugated molecule, (ii) the thioether nature of the connections, and (iii) the presence of mesityl groups is addressed. To this end, a set of spectroscopic tools, such as electron absorption UV−vis−near-IR and Raman, are suitably combined with DFT theoretical calculations in order to get a molecular view of the electronic and molecular structures attained upon *p*-doping or chemical oxidation.

Depending on the chemical constitution and on the level of *p*-doping (equivalent of electrode voltage), these systems are able to easily stabilize radical cations and dications. This could be understood as the potential existence of different input states and a variety of electrical responses through the molecular wire interface, which is of great benefit for storage devices or optical memory elements. It is shown here that the alligator connections of the organic semiconductor to the macroscopic world intervene in the stabilization of the charged species. They should not be regarded as mere contacting elements of the device, since they exert a favorable tuning of the electronic structure of the injected charges. Very large changes are noticed for these terminal sulfur atoms, and it is anticipated that a rehybridization of their atomic orbitals upon charge injection can be expected, which is in agreement with the conclusions by Weiss and co-workers using scanning tunneling microscopy on conjugated molecules anchored to a gold surface via Au−S bonds.[1,2]

The molecular structures generated upon *p*-doping of the single-molecule semiconductor consist of quinoid forms grown at the expense of neutral aromatic structures, which provokes almost full rigidification (planarization) of the scarcely twisted neutral conformation. The quinoidal structures spread on a variable number of thiophene units, depending on the oxidation degree and on the molecular size, starting from the center of the molecule for the radical cation and extending toward the chain ends for the higher oxidation states.

In the case of real systems where molecular wires are connected to metal surfaces,[54−56] there exists a relatively strong perturbation of the molecular properties attributable to the image charges created in the metal electrodes upon hole/electron injection in the molecule. As already stated, the focus of this work does not consider this phenomenon; however, it provides a vibrational analysis of the skeletal CC motions which are

strongly coupled to the π-electron structure. When the electronic overlap between the electrodes and the molecule is weak, single-electron tunneling phenomena are observed. Intriguingly, this electron tunneling process that describes the transport through these nanomolecular systems seems to require a coupling between the molecular electronic levels and some particular vibrational modes. In this regard, our *in-solution* approach already recognizes the existence of vibrational modes strongly coupled to the electronic structure, which seems to correlate with the finding that tunneling in real systems require such electron−vibration coupling.

Acknowledgment. J.C. is grateful to the Ministerio de Ciencia y Tecnología (MCyT) of Spain for a Ramón y Cajal research position of Chemistry at the University of Málaga. R.G.H. thanks the Natural Sciences and Engineering Research Council of Canada for support. The present work was also supported by the Dirección General de Enseñanza Superior (DGES, MEC, Spain) through the research projects BQU2003-03194 and BQU2003-05111. The Junta de Andalucía and the Generalitat Valenciana of Spain are also acknowledged for funding our research groups (FQM-0159 and OCYT-GRUPOS03/173). M.C.R.D. thanks the MEC of Spain for a personal grant.

References and Notes

(1) Donhauser, Z. J.; Mantooth, B. A.; Kelly, K. F.; Bumm, L. A.; Monnell, J. D.; Stapleton, J. J.; Price, D. W., Jr.; Rawlett, A. M.; Allara, D. L.; Tour, J. M.; Weiss, P. S. *Science* **2001**, *292*, 2303.

(2) Donhauser, Z. J.; Mantooth, B. A.; Pearl, T. P.; Kelly, K. F.; Nanayakkara, S. U.; Weiss, P. S. *Jpn. J. Appl. Phys.* **2002**, *41*, 4871.

(3) Tour, J. M. *Acc. Chem. Res*. **2000,** *33*, 791.

(4) Chen, J.; Reed, M. A.; Rawlett, A. M.; Tour, J. M. *Science* **1999**, *286*, 1550.

(5) Reed, M. A.; Zhou, C.; Muller, C. J.; Burgin, T. P.; Tour, J. M. *Science* **1997**, *278*, 252.

(6) Hong, S.; Zhu, J.; Mirkin, C. A. *Science* **1999**, *286*, 523.

(7) Seminario, J. M.; Zacarias, A. G.; Tour, J. M. *J. Am. Chem. Soc*. **1999**, *32*, 6425.

(8) Chen, J.; Reed, M. A.; Rawlett, A. M.; Tour, J. M. *Science* **1999**, *286*, 1550. Fan, F.-R. F.; Yang, J.; Cai, L.; Price, D. W., Jr.; Dirk, S. M.; Kosynkin, D. V.; Yao, Y.; Rawlett, A. M.; Tour, J. M.; Bard, A. J. *J. Am. Chem. Soc.* **2002**, *124*, 5550.

(9) Selzer, Y.; Salomon, A.; Cahen, D. *J. Phys. Chem. B* **2002**, *106*, 10432. Liu, Y.-J.; Yu, H.-Z. *ChemPhysChem* **2003**, *4*, 335.

(10) Xiao, X.; Xu, B.; Tao, N. J. *Nano Lett.* **2004**, *4*, 267.

(11) Ramachandran, G. K.; Hopson, T. J.; Rawlett, A. M.; Nagahara, L. A.; Primak, A.; Lindsay, S. M. *Science* **2003**, *300*, 1413.

(12) Horowitz, G. *Adv. Mater*. **1998**, *10*, 365. Katz, H. E.; Lovinger, A. J.; Johnson, J.; Kloc, C.; Siegrist, T.; Li, W.; Linn, Y. Y.; Dobadalapur, A. *Nature (London)* **2000**, *404*, 478. Bao, Z.; Rogers, J. A.; Katz, H. E. *J. Mater. Chem*. **1999**, *9*, 1895. Fichou, D.; Horowitz, G.; Nishikitani, Y.; Garnier, F. *Chemtronics* **1988**, *3*, 176.

(13) Li, X. C.; Sirringhaus, H.; Garnier, F.; Holmes, A. B.; Moratti, S. C.; Feeder, N.; Clegg, W.; Teat, S. J.; Friend, R. H. *J. Am. Chem. Soc*. **1998**, *120*, 2206. Meng, H.; Bao, Z.; Lovinger, A. J.; Wang, B.; Mujsce, A. M. *J. Am. Chem. Soc*. **2001**, *123*, 9214.

(14) Chesterfield, R. J.; Newman, C. R.; Pappenfus, T. M.; Ewbank, P. C.; Haukaas, M. H.; Mann, K. R.; Miller, L. L.; Frisbie, C. D. *Adv. Mater*. **2003**, *15*, 1278. Pappenfus, T.; Chesterfield, R. J.; Frisbie, C. D.; Mann, K. R.; Casado, J.; Raff, J. D.; Miller, L. L.; Mann, K. R. *J. Am. Chem. Soc.* **2002**, *124*, 4184.

(15) Facchetti, A.; Deng, Y.; Wang, A.; Koide, Y.; Sirringhaus, H.; Marks, T. J.; Friend, R. H. *Angew. Chem., Int. Ed*. **2000**, *39*, 4547. Facchetti, A.; Mushrush, M.; Katz, H. E.; Marks, T. J. *Adv. Mater*. **2003**, *15*, 33. Facchetti, A.; Yoon, M.-H.; Stern, C. L.; Katz, H. E.; Marks, T. J. *Angew. Chem., Int. Ed*. **2003**, *42*, 3900. Facchetti, A.; Yoon, M.-H.; Stern, C. L.; Hutchison, G. R.; Ratner, M. A.; Marks, T. J. *J. Am. Chem. Soc*. **2004**, *126*, 13480. Facchetti, A.; Mushrush, M.; Yoon, M.-H.; Hutchison, G. R.; Ratner, M. A.; Marks, T. J. *J. Am. Chem. Soc*. **2004**, *126*, 13859.

(16) Pasini, M.; Destri, S.; Porzio, W.; Botta, C.; Giovanella, U. *J. Mater. Chem*. **2003**, *13*, 807. Suzuki, M.; Fukuyama, M.; Hori, Y.; Hotta, S. *J. Appl. Phys*. **2002**, *91*, 5706.

(17) Garnier, F.; Yassar, A.; Hajlaoui, R.; Srivastava, P. *Science* **1994**, *265*, 1684.

(18) Garnier, F.; Yassar, A.; Hajlaoui, R.; Horowitz, G.; Deloffre D.; Servet, B.; Ries, S.; Alnot, P. *J. Am. Chem. Soc*. **1993**, *115*, 8716.

(19) See for example: Beebe, J. M.; Engelkes, V. B.; Miller, L. L.; Frisbie, C. D. *J. Am. Chem. Soc.* **2002**, *124*, 11268. Engelkes, V. B.; Beebe, J. M.; Frisbie, C. D. *J. Am. Chem. Soc.* **2004**, *126*, 14287.

(20) Yaliraki, S. N.; Kemp, M.; Ratner, M. A. *J. Am. Chem. Soc*. **1999**, *121*, 3428. Zhou, C.; Deshpande, M. R.; Reed, M. A.; Jones, L.; Tour, J. M. *Appl. Phys. Lett*. **1997**, *71*, 611.

(21) Zerbi, G.; Castiglioni, C.; Del Zoppo, M. In *Electronic Materials: The Oligomer Approach*; Müllen, K., Wegner, G., Eds.; Wiley-VCH: Weinheim, 1998; p 345.

(22) Casado, J.; Hicks, R. G.; Hernández, V.; Myles, D. J. T.; Ruiz Delgado, M. C.; López Navarrete J. T. *J. Chem. Phys.* **2003**, *118*, 1912.

(23) Hernández, V.; Casado, J.; Ramírez, F. J.; Zotti, G.; Hotta, S.; López Navarrete, J. T. *J. Chem. Phys.* **1996**, *104*, 9271.

(24) Castiglioni, C.; Gussoni, M.; López Navarrete, J. T.; Zerbi, G. *Solid State Commun.* **1988**, *65*, 625. López Navarrete, J. T.; Zerbi, G. *J. Chem. Phys.* **1991**, *94*, 957 and 965.

(25) Agosti, E.; Rivola, M.; Hernández, V.; Del Zoppo, M.; Zerbi, G. *Synth. Met*. **1999**, *100*, 101. Del Zoppo, M.; Castiglioni, C.; Zuliani, P.; Zerbi G. In *Handbook of Conducting Polymers*, 2nd ed.; Skotheim, T. A., Elsenbaumer, R. L., Reynolds, J. R., Eds.; Marcel Dekker: New York, 1998; p 765.

(26) Hicks, R. G.; Nodwell, M. B. *J. Am. Chem. Soc*. **2000**, *122*, 6746. For Ph3T and Ph4T, synthetic details have been reported in Hotta S.; Lee, S. A. *Synth. Met.* **1999**, *101*, 551, and Lee, S. A.; Yoshida, Y.; Fukuyama, M.; Hotta S. *Synth. Met.* **1999**, *106*, 39.

(27) Frisch, M. J.; Trucks, G. W.; Schlegel, H. B.; Scuseria, G. E.; Robb, M. A.; Cheeseman, J. R.; Zakrzewski, V. G.; Montgomery, J. A., Jr.; Stratmann, R. E.; Burant, J. C.; Dapprich, S.; Millam, J. M.; Daniels, A. D.; Kudin, K. N.; Strain, M. C.; Farkas, O.; Tomasi, J.; Barone, V.; Cossi, M.; Cammi, R.; Mennucci, B.; Pomelli, C.; Adamo, C.; Clifford, S.; Ochterski, J.; Petersson, G. A.; Ayala, P. Y.; Cui, Q.; Morokuma, K.; Malick, D. K.; Rabuck, A. D.; Raghavachari, K.; Foresman, J. B.; Cioslowski, J.; Ortiz, J. V.; Stefanov, B. B.; Liu, G.; Liashenko, A.; Piskorz, P.; Komaromi, I.; Gomperts, R.; Martin, R. L.; Fox, D. J.; Keith, T.; Al-Laham, M. A.; Peng, C. Y.; Nanayakkara, A.; Gonzalez, C.; Challacombe, M.; Gill, P. M. W.; Johnson, B. G.; Chen, W.; Wong, M. W.; Andres, J. L.; Head-Gordon, M.; Replogle, E. S.; Pople, J. A. *Gaussian 98*, revision A.7; Gaussian, Inc.: Pittsburgh, PA, 1998.

(28) Becke, A. D. *J. Chem. Phys.* **1993**, *98*, 1372.

(29) Stephens, P. J.; Devlin, F. J.; Chabalowski, F. C. F.; Frisch, M. J. *J. Phys. Chem.* **1994**, *98*, 11623.

(30) Novoa, J. J.; Sosa, C. *J. Phys. Chem.* **1995**, *99*, 15837.

(31) Scott, A. P.; Radom, L. *J. Phys. Chem.* **1996**, *100*, 16502.

(32) Rauhut, G.; Pulay, P. *J. Phys. Chem.* **1995**, *99*, 3093.

(33) Francl, M. M.; Pietro, W. J.; Hehre, W. J.; Binkley, J. S.; Gordon, M. S.; Defrees, D. J.; Pople, J. A. *J. Chem. Phys.* **1982**, *77*, 3654.

(34) Runge, E.; Gross, E. K. U. *Phys. Rev. Lett.* **1984**, *52*, 997. Gross, E. K. U.; Kohn, W. *Adv. Quantum Chem.* **1990**, *21*, 255. Gross, E. K. U.; Ullrich, C. A.; Gossmann, U. J. In *Density Functional Theory*; Gross, E. K. U., Driezler, R. M., Eds.; Plenum Press: New York, 1995; p 149.

(35) Casida, M. E. In *Recent Advances in Density Functional Methods, Part I*; Chong, D. P., Ed.; World Scientific: Singapore, 1995; p 115.

(36) Koch, W.; Holthausen, M. C. *A Chemist's Guide to Density Functional Theory*; Wiley-VCH: Weinheim, 2000.

(37) Viruela, P. M.; Viruela, R.; Ortí, E.; Brédas, J.-L. *J. Am. Chem. Soc.* **1997**, *119*, 1360. Viruela, P. M.; Viruela, R.; Ortí, E. *Int. J. Quantum Chem.* **1998**, *70*, 303. Karpfen, A.; Choi, C. H.; Kertesz, M. *J. Phys. Chem. A* **1997**, *101*, 7426.

(38) Orlandi, G.; Zerbetto, F.; Zgierski, M. Z. *Chem. Rev.* **1991**, *91*, 867. Zgierski, M. Z.; Zerbetto, F. *J. Chem. Phys*. **1993**, *99*, 3721.

(39) Negri, F.; Zgierski, M. Z. *J. Chem. Phys.* **1994**, *100*, 2571.

(40) Negri, F.; Zgierski, M. Z. *J. Chem. Phys.* **2001**, *115*, 1298.

(41) Hill, M. G.; Mann, K. R.; Miller, L. L.; Penneau, J. F. *J. Am. Chem. Soc.* **1992**, *114*, 2728. Hill, M. G.; Penneau, J. F.; Zinger, B.; Mann, K. R.; Miller, L. L. *Chem. Mater*. **1992**, *4*, 1106. Miller, L. L.; Yu, Y.; Gunic, E.; Duan, R. *Adv. Mater*. **1995**, *7*, 547. Yu, Y.; Gunic, E.; Zinger, B.; Miller, L. L. *J. Am. Chem. Soc.* **1996**, *118*, 1013. Bauerle, P.; Segelbacher, U.; Maier, A.; Mehring, M. *J. Am. Chem. Soc.* **1993**, *115*, 10217.

(42) Casado, J.; Miller, L. L.; Mann, K. R.; Pappenfus, T. M.; Kanemitsu, Y.; Ortí, E.; Viruela, P. M.; Pou-Amérigo, R.; Hernández, V.; López Navarrete, J. T. *J. Phys. Chem. B* **2002**, *106*, 3872. Casado, J.; Bengoechea, M.; López Navarrete, J. T.; Otero, T. F. *Synth. Met.* **1998**, *95*, 93.

(43) van Haare, J.; Groenendaal, L.; Havinga, E. E.; Janssen, R. A. J.; Meijer, E. W. *Angew. Chem., Int. Ed. Engl.* **1996**, *35*, 638. van Haare, J.; Groenendaal, L.; Havinga, E. E.; Meijer, E. W.; Janssen, R. A. J. *Synth. Met.* **1997**, *85*, 1091.

(44) Levillain, E.; Roncali, J. *J. Am. Chem. Soc.* **1999**, *121*, 8760.

(45) Zotti, G.; Schiavon, G.; Berlin, A.; Pagani, G. *Chem. Mat*. **1993**, *5*, 620.
(46) Cao, J.; Curtis, M. D. *Chem. Mater*. **2003**, *15*, 4424.
(47) Graf, D. D.; Campbell, J. P.; Miller, L. L.; Mann, K. R. *J. Am. Chem. Soc.* **1996**, *118*, 5480.
(48) Campbell, J. P.; Miller, L. L.; Mann, K. R. *J. Am. Chem. Soc.* **1997**, *119*, 5888.
(49) Casado, J.; Miller, L. L.; Mann, K. R.; Pappenfus, T. M.; Hernández, V.; López Navarrete, J. T. *J. Phys. Chem. B* **2002**, *106*, 3597.
(50) Casado, J.; Ruiz Delgado, M. C.; Shirota, Y.; Hernández, V.; López Navarrete, J. T. *J. Phys. Chem. B* **2003**, *107*, 2637.
(51) Albrecht, C. A. *J. Chem. Phys*. **1961**, *34*, 1476.
(52) Horowitz, G. *Solid State Commun*. **1982**, *41*, 729.
(53) Hernández, V.; Casado, J.; Ramírez, F. J.; Zotti, G.; Hotta, S.; López Navarrete, J. T. *J. Chem. Phys.* **1996**, *104*, 9271. Casado, J.; Otero, T. F.; Hotta, S.; Hernández, V.; Ramírez, F. J.; López Navarrete, J. T. *Opt. Mater*. **1998**, *9*, 82.
(54) Zhitenev, N. B.; Meng, H.; Bao, Z. *Phys. Rev. Lett*. **2002**, *88*, 226801.
(55) Prinzbach, H.; Weller, A.; Landenberger, P.; Wahl, F.; Wörth, J.; Scott, L. T.; Gelmont, M.; Olevano, D.; Issendorff, B. *Nature (London)* **2000**, *407*, 60.
(56) Kubatkin, S.; Danilov, A.; Hjort, M.; Cornil, J.; Brédas, J.-L.; Stuhr-Hansen, N.; Hedegård, P.; Bjørnholm, T. *Nature (London)* **2003**, *425*, 698.